Observer-based Composite Super-Twisting Sliding Mode Control for High-Precision Positioning Servo System

1st Xiaoming Wang
College of Automation Engineering,
Shanghai University of Electric Power
Shanghai, China
xm_wang@mail.shiep.edu.cn

2nd Jianliang Mao
College of Automation Engineering,
Shanghai University of Electric Power
Shanghai, China
jl_mao@shiep.edu.cn

3rd Xin Dong
College of Automation Engineering,
Shanghai University of Electric Power
Shanghai, China
dongxin@mail.shiep.edu.cn

4th Chuanlin Zhang
College of Automation Engineering,
Shanghai University of Electric Power
Shanghai, China
clzhang@shiep.edu.cn

2022 China Automation Congress (CAC) | 978-1-6654-6533-5/22/$31.00 ©2022 IEEE | DOI: 10.1109/CAC57257.2022.10055159

***Abstract*—In this paper, an observer-based composite super-twisting sliding mode controller (STSMC) is designed for fast response and enhanced disturbance rejection ability for permanent magnet synchronous motor (PMSM) . Towards this aim, a higher-order sliding mode observer (HOSMO) is first employed for the angular velocity and the lumped disturbance estimation. Subsequently, a novel integral-based terminal sliding mode (ITSM) surface is constructed by introducing the estimated information. Finally, a composite sliding mode controller is derived by integrating the super-twisting algorithm and disturbance feedforward compensation technique. The simulation results fully demonstrate the efficacy of the proposed approach.**

***Index Terms*—super-twisting sliding mode (STSM), integral-based terminal sliding mode (ITSM), higher-order sliding mode observer (HOSMO), permanent magnet synchronous motor (PMSM), position control**

I. Introduction

PMSM has the advantages of low heat generation, low noise, light weight and high efficiency, etc., and has been already widely used in industry. In practical applications, the cascaded PI control approach are usually deployed in PMSM servo system. However, there are usually parametric uncertainties, unmodeled dynamics and uncertain external disturbances in practical servo systems, which will make it difficult to obtain ideal position tracking performance and disturbance rejection ability with PI control methods. As is well known, the high-precision position tracking performance plays a vital role in industry such as electric vehicles [1] and robots [2], therefore, the study of PMSM with high positioning accuracy is of great practical importance.

This work was supported in part by the National Natural Science Foundation of China under Grant 62173221 and Grant 62203292, and in part by the Jiangsu Province Industry-University-Research Collaboration Project under Grant BY2021304. (*Corresponding author: Jianliang Mao.*)

Recently, with the continuous innovation of moderm control theory, many modern control methods have been used in PMSM position control, such as model predictive control (MPC) [3], active disturbance rejection control (ADRC) [4] and sliding mode control (SMC) [5], etc. Among these modern control methodologies, SMC is widely used in nonlinear systems due to its fast response time, robustness to external noise and parameter uptake. However, as we all known, the SMC has inherent chattering drawbacks. In order to weaken chattering, some modified strategies are proposed, such as adaptive SMC [6], STSMC [7], [8], etc. It is notable that the STSMC is commonly employed due to its compensation of disturbances/uncertainties with finite-time convergence of sliding variable. However, for second-order perturbed system, the finite-time convergence of state variables under the traditional linear sliding mode surface control framework can be hardly achieved [8]. In [9], the terminal sliding mode (TSM) surface is deployed to ensure finite-time stability of state variables, but the presence of high frequency switching terms in TSM control will exacerbate undesirable chattering phenomenon [10], [11].

Although the continuous STSMC can weaken system chattering to a certain extent, the control gains are commonly large due to the difficulty in determining the upper bound of the disturbance in PMSM servo system, which will inevitably aggravate the steady state fluctuations. To reduce the impact of uncertainties on system performance, observers are often introduced in practice for disturbance feedforward compensation. For instance, the extended state observer (ESO) is applied in [12], [13] to estimate the states and lumped perturbations synchronously. Nevertheless, ESO can not ensure finite-time convergence, so the nominal performance recovery performance is unavoidably limited. In contrast, the HOSMO is widely employed due to its properties of finite-time

convergence, and accurate estimation of disturbances [14].

To achieve high positioning accuracy of PMSM servo system, the paper proposes a HOSMO-based composite STSMC approach. Firstly, to estimate the accurate state information as well as the lumped disturbance, this paper designs a HOSMO. Furthermore, a new integral-based TSM surface is designed by combining the estimated information. Finally, a composite SMC is developed by incorporating the super-twisting sliding mode reaching law and disturbance feedforwoard compensation. The simulation results show that proposed composite controller can not only ensure finite-time high-precision position tracking, but also has a strong disturbances rejection capability

II. Problem Formulation

It is well known that the mathematical model of three-phase PMSM in $d-q$ axes can be depicted as following [12]

$$\begin{cases} \dot{\theta} = \omega, \\ \dot{\omega} = \dfrac{K_m i_q}{J} - \dfrac{B\omega}{J} - \dfrac{T_L}{J}, \\ \dot{i}_q = -\dfrac{R_s i_q}{L_s} - n_p i_d \omega - \dfrac{n_p \psi_f \omega}{L_s} + \dfrac{u_q}{L_s}, \\ \dot{i}_d = -\dfrac{R_s i_d}{L_s} + n_p i_q \omega - \dfrac{u_d}{L_s} \end{cases} \tag{1}$$

where θ and ω are the position and velocity of the motor, i_d and i_q are the $d-q$ axes currents, u_d and u_q are the $d-q$ axes voltages, J is the rotational inertia, B is the viscous friction coefficient, R_s is the stator resistance, L_s is the stator inductance, n_p is the number of pole pairs, ψ_f is the flux linkage of the motor, respectively, T_L is the external load torque, and $K_m = \frac{3}{2} n_p \psi_f$ is the torque constant.

In this paper, the position-loop control issue is mainly investigated. For the sake of simplifying the system (1), the dynamic equation can be simplified as

$$\ddot{\theta} = b i_q + d(t) \tag{2}$$

where $b = \frac{K_m}{J}$ is the system control gain and $d(t) = -\frac{B\omega}{J} - \frac{T_L}{J}$ is regarded as the lumped disturbance term.

To proceed, the position we want the PMSM to reach is θ_r, and then the position tracking error can be denoted by $x_1 = \theta_r - \theta$. Subsequently, by defining the q-axis current i_q as the system input u, the state-space model of the PMSM can be formulated as

$$\begin{cases} \dot{x}_1 = x_2, \\ \dot{x}_2 = \ddot{\theta}_r - bu - d(t), \\ y = x_1. \end{cases} \tag{3}$$

III. HOSMO-base STSMC Design

In this section, a composite SMC integrated with HOSMO and a ITSM surface is designed, and the design procedure is presented step by step.

A. Design of HOSMO

For system (3), only the x_1 is known. To obtain the accurate auxiliary state variable x_2 and the lumped disturbance $d(t)$, the HOSMO is designed as

$$\begin{cases} \dot{\hat{x}}_1 = \hat{x}_2 + z_1, \\ \dot{\hat{x}}_2 = \hat{x}_3 + \ddot{\theta}_r - bu + z_2, \\ \dot{\hat{x}}_3 = z_3 \end{cases} \tag{4}$$

where $\hat{x}_1, \hat{x}_2$ are the estimations of the state variable x_1, x_2, and $\hat{x}_3$ is the lumped disturbance, respectively, z_1, z_2, z_3 are the correction terms, which are defined as the following relationships with

$$\begin{cases} z_1 = \mu_1 |e_1|^{2/3} \mathrm{sign}(e_1), \\ z_2 = \mu_2 |e_1|^{1/3} \mathrm{sign}(e_1), \\ z_3 = \mu_3 \mathrm{sign}(e_1) \end{cases} \tag{5}$$

where $e_1 = x_1 - \hat{x}_1$ is the estimation error and μ_1, μ_2, μ_3 are the observer gains.

In what follows, the rests of error variables are denoted as $e_2 = x_2 - \hat{x}_2$, $e_3 = d(t) - \hat{x}_3$. Combining with Eqs. (4)-(5), the HOSMO for the angular velocity and the lumped disturbance estimation is derived as

$$\begin{cases} \dot{\hat{x}}_1 = \hat{x}_2 + \mu_1 |e_1|^{2/3} \mathrm{sign}(e_1), \\ \dot{\hat{x}}_2 = \hat{x}_3 + \ddot{\theta}_r - bu + \mu_2 |e_1|^{1/3} \mathrm{sign}(e_1), \\ \dot{\hat{x}}_3 = \mu_3 \mathrm{sign}(e_1). \end{cases} \tag{6}$$

Furthermore, the observer error model can be written as

$$\begin{cases} \dot{e}_1 = -\mu_1 |e_1|^{2/3} \mathrm{sign}(e_1) + e_2, \\ \dot{e}_2 = -\mu_2 |e_1|^{1/3} \mathrm{sign}(e_1) + e_3, \\ \dot{e}_3 = -\mu_3 \mathrm{sign}(e_1) + \dot{d}(t). \end{cases} \tag{7}$$

Assume that the lumped disturbance $d(t)$ is a Lipschitz function and $|\dot{d}(t)| < \Delta$. It follows from [8] that as long as the appropriate parameters μ_1, μ_2, μ_3 are chosen then the system will converge in finite time, i.e., there is a finite-time constant T_0, $\forall t \geq T_0$, $e_i \equiv 0$ and $\forall t < T_0$, $|e_i| \leq E_i^{\max}$, which ensures that $x_1 = \hat{x}_1$, $x_2 = \hat{x}_2$, $d(t) = \hat{x}_3$ in a finite-time constant T_0.

B. Composite STSMC Construction

This section will present the design procedure of the composite STSMC strategy by combining the states estimation derived from HOSMO.

To begin with, an ITSM surface is designed as

$$\hat{s} = \hat{x}_2 + \int_0^t \left[k_1 |x_1|^{\alpha} \mathrm{sign}(x_1) + k_2 |\hat{x}_2|^{\beta} \mathrm{sign}(\hat{x}_2) \right] \mathrm{d}\tau \tag{8}$$

where $\alpha = \beta/(2-\beta)$, $\beta \in (1-\xi, 1)$, $\xi \in (0,1)$, $k_1, k_2 > 0$.

Then the derivative for the above ITSM surface $\hat{s}$ is obtained

$$\begin{aligned} \dot{\hat{s}} = {} & \hat{x}_3 + \ddot{\theta}_r - bu + k_1 |x_1|^{\alpha} \mathrm{sign}(x_1) + k_2 |\hat{x}_2|^{\beta} \mathrm{sign}(\hat{x}_2) \\ & + \mu_2 |e_1|^{1/3} \mathrm{sign}(e_1). \end{aligned} \tag{9}$$

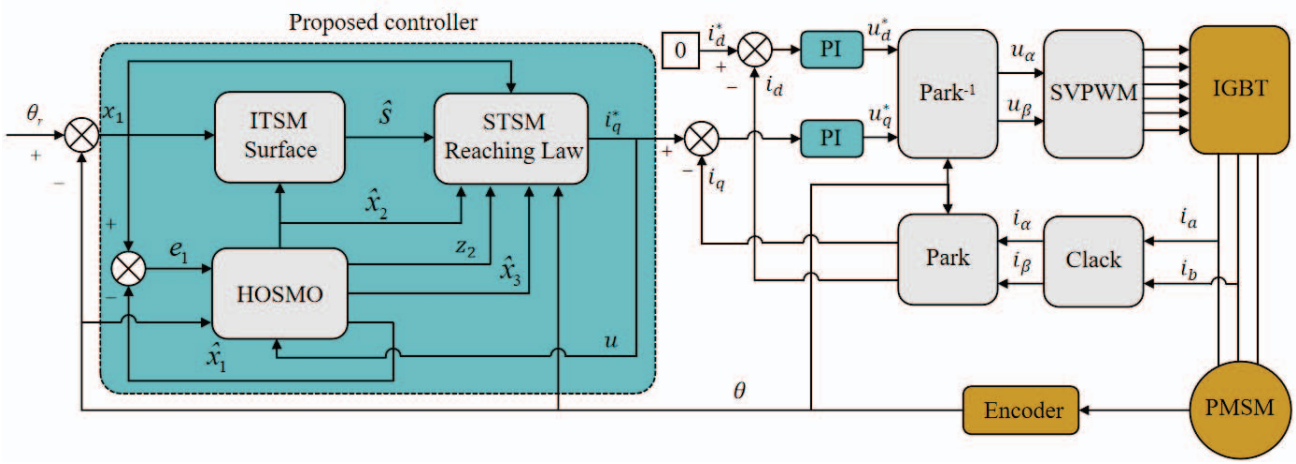

Fig. 1. Block diagram of the composite STSMC strategy.

To ensure that the $\hat{s}$ and $\dot{\hat{s}}$ can converge, a finite-time controller u is necessary to introduced. To this aim, we set $\dot{\hat{s}} = 0$ in Eq. (9), and the controller u_{eq} can be derived as

$$u_{eq} = b^{-1}\Big[\ddot{\theta}_r + k_1|x_1|^{\alpha}\mathrm{sign}(x_1) + k_2|\hat{x}_2|^{\beta}\mathrm{sign}(\hat{x}_2) + \mu_2|e_1|^{1/3}\mathrm{sign}(e_1) + \hat{x}_3\Big]. \tag{10}$$

Furthermore, aiming to ensure finite-time convergence and weaken the chattering, the STSM algorithm is introduced for the reaching law design, that is

$$u_{sta} = b^{-1}\left[\lambda_1|\hat{s}|^{1/2}\mathrm{sign}(\hat{s}) + \lambda_2\int_0^t \mathrm{sign}(\hat{s})\mathrm{d}\tau\right] \tag{11}$$

where $\lambda_1, \lambda_2 > 0$ are the control gains.

Finally, combining Eqs. (10) and (11), the proposed composite STSMC is derived as

$$\begin{aligned} u &= u_{eq} + u_{sta} \\ &= b^{-1}\Big[\ddot{\theta}_r + \mu_2|e_1|^{1/3}\mathrm{sign}(e_1) + \hat{x}_3 + k_1|x_1|^{\alpha}\mathrm{sign}(x_1) \\ &\quad + k_2|\hat{x}_2|^{\beta}\mathrm{sign}(\hat{x}_2) + \lambda_1|\hat{s}|^{1/2}\mathrm{sign}(\hat{s}) + \lambda_2\int_0^t \mathrm{sign}(\hat{s})\mathrm{d}\tau\Big]. \end{aligned} \tag{12}$$

The block diagram of composite STSMC strategy is shown in Fig. 1.

C. Stability Analysis of the composite STSMC

In order to demonstrate the theoretical validity of the proposed control method, stability analysis of the proposed STSMC is performed in this section. To simplify the proof process of the designed STSMC, the following important lemmas are first introduced.

Lemma 1: [7] For the following systems

$$\begin{cases} \dot{x}_1 = -\lambda_1|x_1|^{1/2}\mathrm{sign}(x_1) + x_2, \\ \dot{x}_2 = -\lambda_2\mathrm{sign}(x_1) \end{cases} \tag{13}$$

if the parameters λ_1, λ_2 are chosen positively, the system state x_1 and x_2 will converges finite time to zero, where the finite time constant T satisfies

$$T \le \frac{2\lambda_{\max}\{P\}}{\lambda_{\min}^{1/2}\{P\}\lambda_{\min}\{Q\}}V^{1/2}(x_1(0)) \tag{14}$$

where $V = \zeta^{\mathrm{T}}P\zeta$ is the Lyapunov function, P and Q are positive definite matrices, satisfying $\zeta = \left[|x_1|^{1/2}\mathrm{sign}(x_1), x_2\right]^{\mathrm{T}}$, $P = \begin{bmatrix} \lambda_1^2 + 4\lambda_2 & \lambda_1 \\ \lambda_1 & 2 \end{bmatrix}$, $Q = \begin{bmatrix} \lambda_1^2 + 2\lambda_2 & \lambda_1 \\ \lambda_1 & 1 \end{bmatrix}$.

Lemma 2: [10] For a dynamic system of dimension n

$$\dot{x}_1 = x_2,\ \cdots,\ \dot{x}_{n-1} = x_n,\ \dot{x}_n = u \tag{15}$$

system (15) is finite-time convergence if the control law satisfies

$$u = -\kappa_1|x_1|^{\alpha_1}\mathrm{sign}(x_1) - \cdots - \kappa_n|x_n|^{\alpha_n}\mathrm{sign}(x_n) \tag{16}$$

where $\alpha_{i-1} = \frac{\alpha_i\alpha_{i+1}}{2\alpha_{i+1}-\alpha_i}(i = 2, \ldots, n)$, $\alpha_{n+1} = 1$, $\alpha_n = \alpha$ in which α belongs to an interval $(1-\xi, 1)$, $\xi > 0$, and $\kappa_1, \ldots, \kappa_n > 0$ should be selected such that polynomial $\lambda^n + \kappa_n\lambda^{n-1} + \ldots + \kappa_2\lambda + \kappa_1$ is Hurwitz.

Proof: The stability analysis is performed in the following steps. First, it is shown that the designed ITSM surface $\hat{s}$ can converge in finite time. Second, it is shown that the state variables $\hat{s}$, x_1, and $\hat{x}_2$ are bounded in finite time $[0, T_0]$. Finally, it is shown that the state variable x_1, i.e., the position tracking error can converge in finite-time.

Step 1: ITSM surface finite time convergence. First, substituting the designed control law (12) into Eq. (9) yields

$$\dot{\hat{s}} = -\lambda_1|\hat{s}|^{1/2}\mathrm{sign}(\hat{s}) - \lambda_2\int_0^t \mathrm{sign}(\hat{s})\mathrm{d}\tau. \tag{17}$$

According to Lemma 1, it is observed that the designed controller can guarantee converge in finite time of the ITSM surface, i.e., there exists a finite-time constant T_1, $\forall t \ge T_1$, $\hat{s} \equiv \dot{\hat{s}} \equiv 0$.

Step 2: State variables finite time bounded. Construct a finite-time bounded function as

$$V(\hat{s}, x_1, \hat{x}_2) = \frac{1}{2}(\hat{s}^2 + {x_1}^2 + \hat{x}_2^2). \tag{18}$$

By substituting the STSMC (12) into Eq. (6) yields

$$\begin{aligned}\dot{\hat{x}}_2 = &-k_1|x_1|^{\alpha}\mathrm{sign}(x_1) - k_2|\hat{x}_2|^{\beta}\mathrm{sign}(\hat{x}_2)\\ &- \lambda_1|\hat{s}|^{1/2}\mathrm{sign}(\hat{s}) - \lambda_2\int_0^t \mathrm{sign}(\hat{s})\mathrm{d}\tau.\end{aligned} \tag{19}$$

Taking the derivative of V along Eqs. (17) and (19) yields

$$\begin{aligned}\dot{V} &= -\hat{s}\left[\lambda_1|\hat{s}|^{1/2}\mathrm{sign}(\hat{s}) + \lambda_2\int_0^t \mathrm{sign}(\hat{s})\mathrm{d}\tau\right] + x_1(\hat{x}_2 + e_2)\\ &\quad - \hat{x}_2\left[k_1|x_1|^{\alpha}\mathrm{sign}(x_1) + k_2|\hat{x}_2|^{\beta}\mathrm{sign}(\hat{x}_2)\right.\\ &\qquad \left. + \lambda_1|\hat{s}|^{1/2}\mathrm{sign}(\hat{s}) + \lambda_2\int_0^t \mathrm{sign}(\hat{s})\mathrm{d}\tau\right]\\ &\le \frac{\lambda_1}{2}\hat{s}^2 + \frac{1 + k_1 + |e_2|}{2}{x_1}^2 + \frac{1 + 2k_1 + 2\lambda_1 + \lambda_2}{2}\hat{x}_2^2\\ &\quad + \frac{k_1 + |e_2| + \lambda_1 + \lambda_2 t^2}{2}\\ &\le \mathcal{K}V_b + \mathcal{L}(t)\end{aligned} \tag{20}$$

where $\mathcal{K} = \frac{1}{2}\max\{\lambda_1, 1 + k_1 + E_2^{\max}, 1 + 2k_1 + 2\lambda_1 + \lambda_2\}$, $\mathcal{L}(t) = \frac{1}{2}(k_1 + E_2^{\max} + \lambda_1 + \lambda_2 t^2)$.

By solving Eq. (20) in the time interval $[0, T_0]$, we have $V_b \le \mathcal{L}(T_0)/\mathcal{K} + (V_b(0) - \mathcal{L}(T_0)/\mathcal{K})e^{\mathcal{K}t}$, which shows that the state variables $\hat{s}, x_1, \hat{x}_2$ will be bounded for a finite period of time T_0.

Step 3: Position tracking error finite time convergence. Taking the derivative of ITSM surface of Eq. (8) yields

$$\dot{\hat{s}} = \dot{\hat{x}}_2 + k_1|x_1|^{\alpha}\mathrm{sign}(x_1) + k_2|\hat{x}_2|^{\beta}\mathrm{sign}(\hat{x}_2) \tag{21}$$

Define a time constant $T = \max\{T_0, T_1\}$. When $t \in [T, \infty)$, one obtains $\hat{s} = \dot{\hat{s}} = 0$ and $\hat{x}_2 = x_2$, then system (21) can be further reduced to

$$\dot{x}_2 = -k_1|x_1|^{\alpha}\,\mathrm{sign}(x_1) - k_2|x_2|^{\beta}\,\mathrm{sign}(x_2). \tag{22}$$

According to Lemma 2, we can obtain that the position tracking error x_1 can converge in finite time.

It can be seen that, for the PMSM system (3), the composite STSMC (12) designed in this paper which includes HOSMO (6), ITSM surface (8), STSM reaching law(11), and tracking error x_1 can ensure finite time stability

IV. Simulation Analysis

To verify the efficacy of the HOSMO-based composite STSMC proposed in the paper, this chapter is simulated and verified in MATLAB/Simulink. The parameters of PMSM are listed in Table I. To further illustrate the superiority of the proposed controller, this section compares the proposed controller with the following candidate controllers in terms of both dynamic response and anti-disturbances ability with a system sampling period of 100μs. The two control algorithms used for comparison are as follows:

TABLE I
PMSM Parameters

Parameters	Symbols&Units	Values
Stator resistance	$R_s(\Omega)$	0.36
Phase inductance	$L(mH)$	0.2
Number of poles	n_p	4
Rotational inertia	$J(10^{-6}kg\cdot m^2)$	7.06
Flux linkage	$\Psi(W_b)$	0.0064
Friction coefficient	$B(N\cdot s/m)$	2.64
Rated speed	$n_N(rpm)$	4107
Rated current	$I_N(A)$	7.1
DC bus supply voltage	$V_b(V)$	24

1) STSM-ESO: The ESO-based STSMC approach in [13] is designed as

$$\begin{cases}\dot{\hat{x}}_1 = \hat{x}_2 - \mu_1 e_1,\\ \dot{\hat{x}}_2 = \hat{x}_3 - \mu_2 e_1 + \ddot{\theta}_r - bu,\\ \dot{\hat{x}}_3 = -\mu_3 e_1,\\ \hat{s} = cx_1 + \hat{x}_2,\\ u = b^{-1}\left[\ddot{\theta}_r + c\hat{x}_2 + \lambda_1|\hat{s}|^{1/2}\mathrm{sign}(\hat{s}) + \lambda_2\int_0^t \mathrm{sign}(\hat{s})\mathrm{d}\tau\right]\end{cases} \tag{23}$$

where c is the sliding mode surface gain and μ_1, μ_2, μ_3 are the observer gains.

2) NFTSM-HOSMO: The HOSMO-based nonsingular fast TSM control method in [14] is designed as

$$\begin{cases}\dot{\hat{x}}_1 = \hat{x}_2 + \mu_1|e_1|^{2/3}\mathrm{sign}(e_1),\\ \dot{\hat{x}}_2 = \hat{x}_3 + \ddot{\theta}_r - bu + \mu_2|e_1|^{1/3}\mathrm{sign}(e_1),\\ \dot{\hat{x}}_3 = \mu_3\mathrm{sign}(e_1),\\ \hat{s} = x_1 + \alpha|x_1|^{\sigma_1}\mathrm{sign}(x_1) + \beta|\hat{x}_2|^{\sigma_2}\mathrm{sign}(\hat{x}_2),\\ u = b^{-1}\left[\ddot{\theta}_r + \dfrac{|\hat{x}_2|^{2-\sigma_2}\mathrm{sign}(\hat{x}_2)}{\beta\sigma_2}(1 + \alpha\sigma_1|x_1|^{\sigma_1}) + \hat{x}_3\right.\\ \left. + \mu_2|e_1|^{1/3}\mathrm{sign}(e_1) + \lambda_1|\hat{s}|^{1/2}\mathrm{sign}(\hat{s}) + \lambda_2\int_0^t \mathrm{sign}(\hat{s})\mathrm{d}\tau\right]\end{cases} \tag{24}$$

where $\alpha, \beta, \sigma_1, \sigma_2$ are the sliding mode surface gains.

The controller gain parameters that appear in this paper are shown in Table II.

TABLE II
Controller Parameters

Controllers	Parameters
STSM-ESO	$c = 30, \mu_1 = 3\times 1000,$ $\mu_2 = 3\times 1000^2, \mu_3 = 1000^3,$ $\lambda_1 = 600, \lambda_2 = 1000$
NFTSM-HOSMO	$\alpha = 500, \beta = 1, \sigma_1 = 5/3, \sigma_2 = 7/5,$ $\mu_1 = 30\times 2000^{\frac{1}{3}}, \mu_2 = 800\times 2000^{\frac{1}{2}},$ $\mu_3 = 600\times 2000, \lambda_1 = 600, \lambda_2 = 1000$
Proposed	$k_1 = 12000, k_2 = 510, \xi = 0.65,$ $\mu_1 = 30\times 2000^{\frac{1}{3}}, \mu_2 = 800\times 2000^{\frac{1}{2}},$ $\mu_3 = 600\times 2000, \lambda_1 = 600, \lambda_2 = 1000$

Remark 1: To ensure the fairness of the simulation results, the FOC strategy with $i_d = 0$ is used for all three sets of

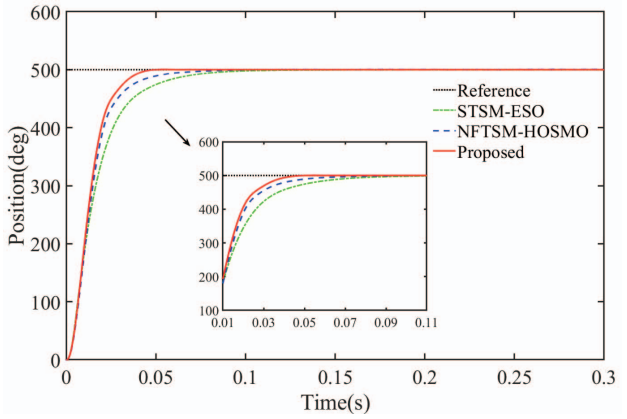

Fig. 2. Position response curves in case of step signal tracking.

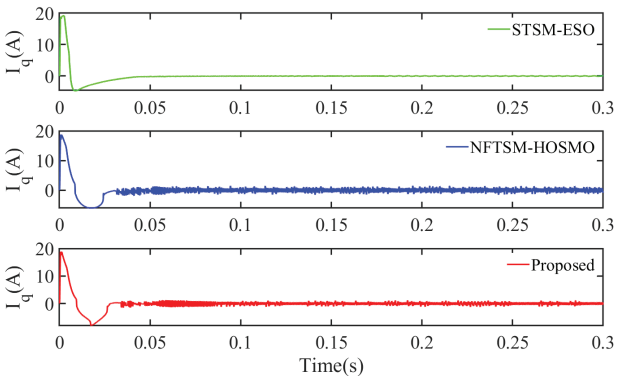

Fig. 3. Current response curves in case of step signal tracking.

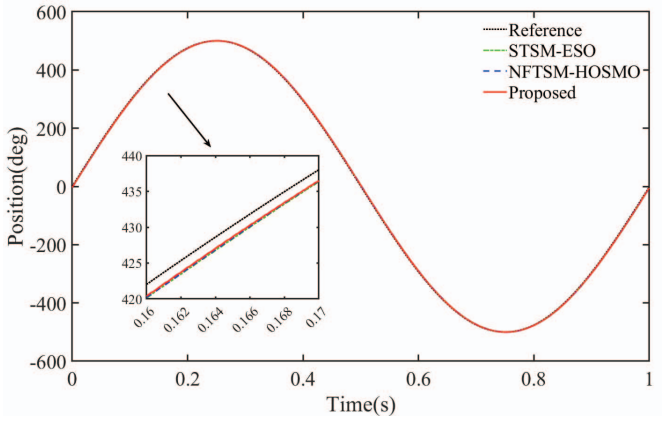

Fig. 4. Position response curves in case of sinusoidal signal tracking.

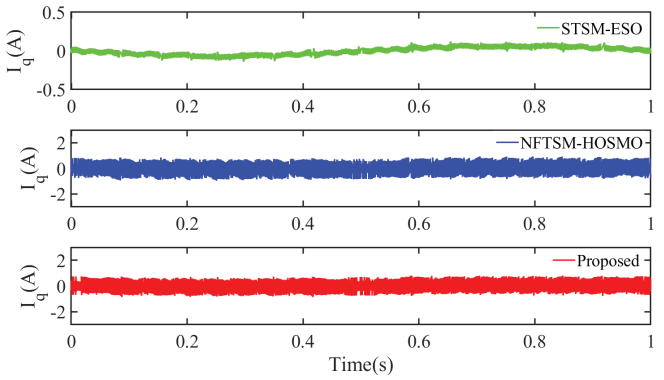

Fig. 5. Current response curves in case of sinusoidal signal tracking.

current loops, and the PI controller with a sampling period of 50μs is used for $d-q$ axes currents with the same parameters.

A. Dynamic Response Performance

To demonstrate that the proposed composite STSMC controller has superior dynamic response performance, a step signal with a desired position of 500 degrees and a sinusoidal signal with an amplitude of 500 degrees and a period of 1s are given, respectively.

It follows from Figs. 2 and 4 that the proposed composite STSMC has better transient performance among the three control methods. Meanwhile, Figs. 3 and 5 show that although the utilization of HOSMO and TSM surface has a larger current ripple, it does not affect the position control accuracy. This is essentially due to the non-smooth nature of the proposed control approach with continuous control action.

B. Disturbance Rejection Ability

To verify the disturbance rejection ability, a constant load disturbance of 0.1 N·m (37% of rated torque) is applied at 1.1s and a sinusoidal load disturbance with an amplitude of 0.3 N·m and a period of 1s is applied at 2.5s in case of step signal tracking, respectively.

From Figs. 6 and 8, we can clearly see that the proposed composite STSMC has stronger disturbance rejection performance and faster recovery time after imposing external load torque. Especially for time-varying disturbances, it is obvious that be seen from Fig. 8 that HOSMO has significantly better anti-disturbance ability than ESO due to its finite-time convergence property. Meanwhile, Figs. 7 and 9 show the estimated values of the two observers.

V. Conclusion

For the dynamic response and disturbance rejection performance of the PMSM servo system, the composite STSMC proposed in this paper has significantly improved it. By introducing HOSMO, an output-based second-order STSM has been essentially realized. Stability analysis proves that the designed STSMC can guarantee the finite-time convergence of the system state variables. Simulations have verified the advantages of the proposed STSMC method in terms of both position tracking accuracy and robustness against disturbances, and chattering is alleviated to some extent.

References

[1] J. Lara, J. Xu and A. Chandra, "Effects of rotor position error in the performance of field-oriented-controlled PMSM drives for electric vehi-

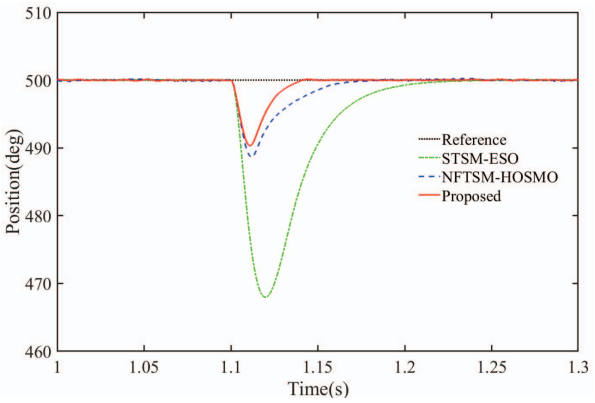

Fig. 6. Disturbance rejection in case of step signal tracking with constant load disturbance imposed.

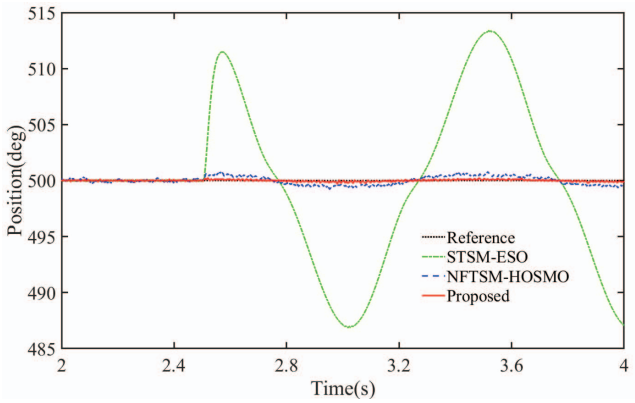

Fig. 8. Disturbance rejection in case of step signal tracking with sinusoidal load disturbance imposed.

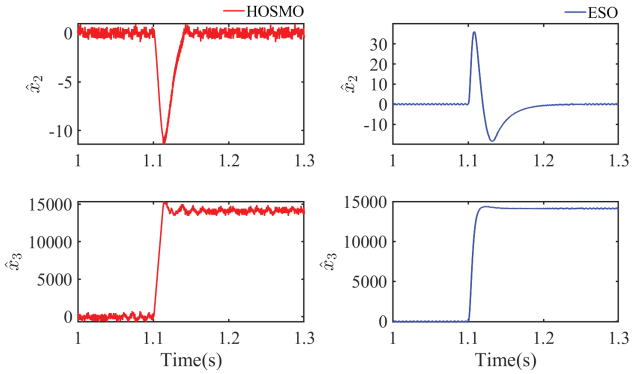

Fig. 7. Observation results in case of step signal tracking with constant load disturbance imposed.

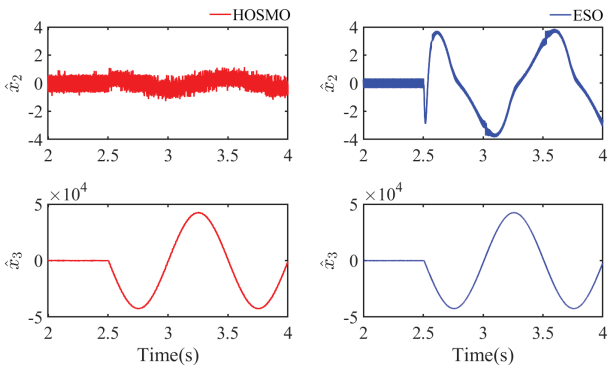

Fig. 9. Observation results in case of step signal tracking with sinusoidal load disturbance imposed.

cle traction applications," *IEEE Transactions on Industrial Electronics*, vol. 63, no. 8, pp. 4738-4751, 2016.

[2] A. Wang, Q. Zhang and Q. Ye, "Vector control strategy for PMSM using rotor kinetic energy," *2016 IEEE 11th Conference on Industrial Electronics and Applications (ICIEA)*, pp. 1525-1529, 2016.

[3] Z. Mynar, L. Vesely and P. Vaclavek, "PMSM model predictive control with field-weakening implementation," *IEEE Transactions on Industrial Electronics*, vol. 63, no. 8, pp. 5156-5166, 2016.

[4] P. Lin, Z. Wu, K. Liu and X. Sun, "A class of linear–nonlinear switching active disturbance rejection speed and current controllers for PMSM," *IEEE Transactions on Power Electronics*, vol. 36, no. 12, pp. 14366-14382, 2021.

[5] X. Sun, H. Yu and X. Liu, "Design and Application of Sliding Mode Controller in PMSM Position Tracking Control Based on Adaptive Backstepping," *2018 Chinese Automation Congress (CAC)*, pp. 3507-3511, 2018.

[6] Y. Chen, B. Cai and G. Cui, "The Design of Adaptive Sliding Mode Controller Based on RBFNN Approximation for Suspension Control of MVAWT," *2020 Chinese Automation Congress (CAC)*, pp. 1080-1084, 2020.

[7] J. Mao, S. Li, Q. Li and J. Yang, "Continuous second-order sliding mode control based on disturbance observer for LOS stabilized system," *2016 14th International Workshop on Variable Structure Systems (VSS)*, pp. 394-399, 2016.

[8] A. Chalanga, S. Kamal, L. Fridman, B. Bandyopadhyay and J. Moreno, "Implementation of super-twisting control: super-twisting and higher order sliding-mode observer-based approaches," *IEEE Transactions on Industrial Electronics*, vol. 63, no. 6, pp. 3677-3685, 2016.

[9] Y. Feng, X. Yu, and Z. Man, "Non-singular terminal sliding mode control of rigid manipulators," *Automatica*, vol. 38, no. 12, pp.2159-2167, 2002.

[10] J. Mao, J. Yang, X. Liu, S. Li and Q. Li, "Modeling and robust continuous TSM control for an inertially stabilized platform with couplings," *IEEE Transactions on Control Systems Technology*, vol. 28, no. 6, pp. 2548-2555, 2020.

[11] J. Yang, S. Li, J. Su, and X. Yu, "Continuous nonsingular terminal sliding mode control for systems with mismatched disturbances," *Automatica*, vol. 49, no.7, pp. 2287-2291, 2013.

[12] Q. Hou and S. Ding, "Finite-time extended state observer-based super-twisting sliding mode controller for PMSM drives with inertia identification," *IEEE Transactions on Transportation Electrification*, vol. 8, no. 2, pp. 1918-1929, 2022.

[13] C. Ren, X. Li, X.Yang and S. Ma, "Extended state observer-based sliding mode control of an omnidirectional mobile robot with friction compensation," *IEEE Transactions on Industrial Electronics*, vol. 66, no. 12, pp. 9480-9489, 2019.

[14] D. Xu, B. Ding, B. Jiang, W. Yang and P. Shi, "Nonsingular fast terminal sliding mode control for permanent magnet linear synchronous motor via high-order super-twisting observer," *IEEE/ASME Transactions on Mechatronics*, vol. 27, no. 3, pp. 1651-1659, 2022.